ACS APPLIED MATERIALS & INTERFACES

Research Article

Cite This: ACS Appl. Mater. Interfaces 2018, 10, 2810−2818

www.acsami.org

High Yield Exfoliation of WS_2 Crystals into 1−2 Layer Semiconducting Nanosheets and Efficient Photocatalytic Hydrogen Evolution from WS_2/CdS Nanorod Composites

Danyun Xu,[†] Pengtao Xu,[‡] Yuanzhi Zhu,[†] Wenchao Peng,[†] Yang Li,[†] Guoliang Zhang,[†] Fengbao Zhang,[†] Thomas E. Mallouk,*[,‡] and Xiaobin Fan*[,†]

[†]School of Chemical Engineering and Technology, State Key Laboratory of Chemical Engineering, Collaborative Innovation Center of Chemical Science and Engineering, Tianjin University, Tianjin 300072, China

[‡]Departments of Chemistry, Biochemistry and Molecular Biology, Physics, and Center for 2-Dimensional and Layered Materials, The Pennsylvania State University, University Park, Pennsylvnia 16802, United States

Supporting Information

ABSTRACT: Monolayer WS_2 has interesting properties as a direct bandgap semiconductor, photocatalyst, and electrocatalyst, but it is still a significant challenge to prepare this material in colloidal form by liquid-phase exfoliation (LPE). Here, we report the preparation of 1−2 layer semiconducting WS_2 nanosheets in a yield of 18−22 wt % by a modified LPE method that involves preintercalation with substoichiometric quantities of *n*-butyllithium. The exfoliated WS_2 nanosheeets are n-type, have a bandgap of ∼1.78 eV, and act as a cocatalyst with CdS nanorods in photocatalytic hydrogen evolution using lactate as a sacrificial electron donor. Up to a 26-fold increase in H_2 evolution rate was observed with WS_2/CdS hybrids compared with their pure CdS counterpart, and an absorbed photon quantum yield (AQE) of >60% was measured with the optimized photocatalyst.

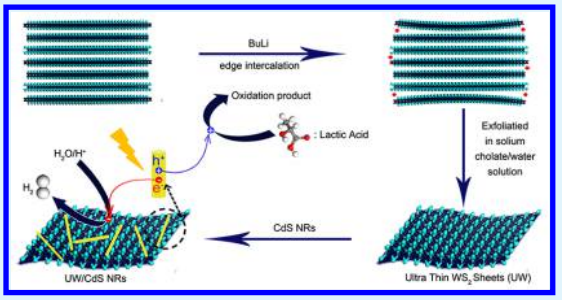

KEYWORDS: *liquid-phase exfoliation, 1−2 layer semiconducting WS_2 nanosheets, preintercalation, cocatalyst, photocatalytic hydrogen evolution*

INTRODUCTION

Over the past decade, the remarkable properties of single-layer graphene[1,2] have stimulated renewed interest in two-dimensional nanomaterials,[3−5] especially the transition metal dichalcogenides (TMDs).[5,6] TMDs are layered compounds in which the metal atoms are sandwiched between close-packed chalcogenide planes, and their bulk crystals thus consist of stacks of three atom-thick sheets. Because the sheets are held together by largely noncovalent interactions, TMD crystals can be exfoliated into mono- or few layered nanosheets by both chemical and physical methods. Unlike graphene, which is a zero-bandgap material, some TMD nanosheets have intrinsic semiconducting characteristics and thus have promise for utilization in optoelectronic devices, thin film transistors, and solar energy conversion.[7−12] Among these compounds, WS_2 and MoS_2 have been most widely studied because their bandgaps are nearly optimal for solar photoconversion and because they are good catalysts for the hydrogen evolution reaction.[13−16]

At present, the lithium intercalation method, normally involving nonaqueous lithium intercalation followed by a water exfoliation step, is the oldest and most popular method for preparing exfoliated WS_2 and MoS_2.[17−20] However, an undesirable phase conversion from the semiconducting 2H to the metallic 1T (trigonal-antiprismatic) phase occurs upon intercalation to form $LiMoS_2$ or $LiWS_2$.[20−22] Although the recovery of the 2H (or 1H for monolayer)[23] phase can be realized by annealing or irradiation of the 1T phase,[17,18,24,25] abundant vacancy defects and lattice distortions are observed in the exfoliated nonosheets.[21] The micromechanical exfoliation method,[26] which produces high-quality nanosheets without the 2H → 1T phase conversion, is not scalable to applications that require bulk quantities of material. Therefore, sonication[27,28] or shear mixing[29,30] assisted liquid-phase exfoliation (LPE) is typically used, not only because of the low defect density of the resulting semiconducting nanosheets but also because of simple processability and potentially low cost.

Normally, LPE can be achieved in solvents with appropriate surface tension.[27,31−33] For example, a number of high-boiling organic solvents, especially *N*-methyl-2-pyrrolidone and other pyrrolidone-based solvents, have been found to be compatible with MoS_2 exfoliation.[27,28,34] Effective LPE can be also achieved in aqueous media with a range of surfactants, proteins, and polymers.[35−38] However, the LPE strategy suffers from a low yield of single- or few-layer products. Recently, we and other groups have found that the exfoliation of MoS_2 or other TMDs

Received: October 14, 2017
Accepted: January 5, 2018
Published: January 5, 2018

DOI: 10.1021/acsami.7b15614
ACS Appl. Mater. Interfaces 2018, 10, 2810−2818

can be significantly improved by intercalation, preintercalation, or oxidation at the edges of the bulk crystals.[28,39−42] However, it is still a formidable challenge to exfoliate bulk crystals of 2H-WS_2 by LPE into monolayer products, which have a direct band gap and promising applications in photocatalysis.[8,43−46]

In this study (Scheme 1), we demonstrate that 1−2 layer 2H-WS_2 nanosheets can be directly exfoliated from WS_2 crystals

Scheme 1. Illustration for 1-2 Layered 2H-WS_2 Preparation and Its Application as Co-catalyst for Photocatalytic Hydrogen Evolution

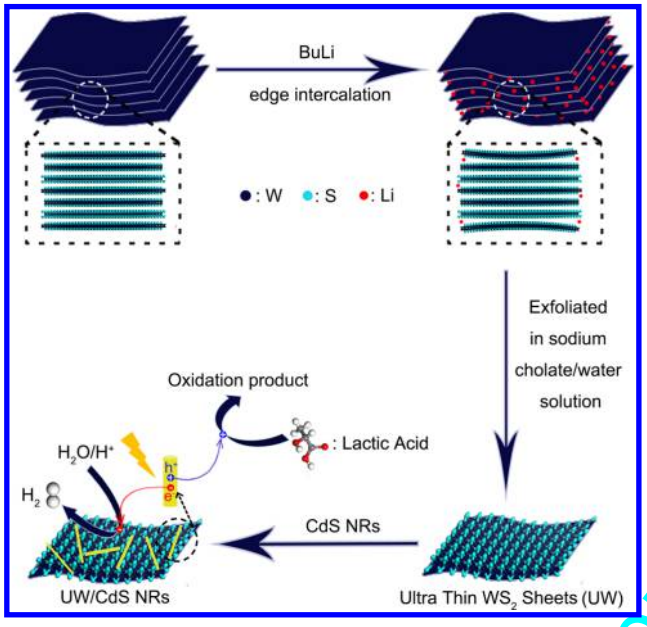

after preintercalation with substoichiometric amounts of lithium, with record high yield of 18−22 wt %. The properties of these nanosheets as a cocatalyst for photocatalytic hydrogen evolution were also investigated. Exfoliation is found to dramatically increase the H_2 evolution rate and absorbed photon quantum yield in WS_2/CdS nanorod hybrids relative to their pure CdS counterpart.

RESULTS AND DISCUSSION

Density Functional Theory Calculations. As we previously reported for the preparation of MoS_2,[41] the preintercalation of WS_2 crystals was achieved by reaction with substoichiometric *n*-butyllithium. However, because of the greater difficulty of WS_2 intercalation, larger quantities of *n*-butyllithium were used, and the reaction was carried out at 50 °C.[47] Density functional theory (DFT) calculations revealed that at low Li content, the formation energy of the 2H phase Li_xWS_2 (normalized per Li atom) with different stage structures are all energetically favored over their 1T phase counterparts (Figure 1). For example, the formation energy of the first-stage 1T phase of $Li_{0.5}WS_2$ is calculated to be 46.4 kJ/mol higher than that of its 2H phase counterpart (Figure S1), although this conclusion is valid only at thermodynamic equilibrium for an ordered distribution of Li atoms. Experimentally, we detected very little of the 1T phase by using X-ray photoelectron spectroscopy (XPS) when substoichiometric *n*-butyllithium (x = Li/W ≤ 0.35) was used (see the Supporting Information, Figure S2). Therefore, the $Li_{0.35}WS_2$ compound was chosen for subsequent exfoliation experiments.

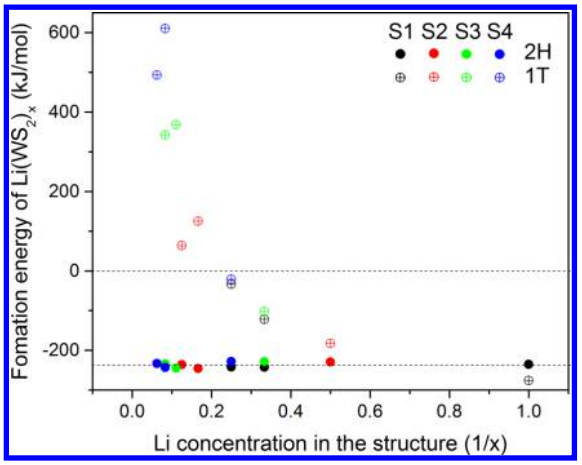

Figure 1. Formation energy of $Li(WS_2)_x$ at different Li stoichiometries. S1, S2, S3, and S4 mean the stage 1, stage 2, stage 3, and stage 4 intercalation. Solid circles denote the 2H structure while the hollow circles denote the 1T structure. DFT calculations are further explained in the Supporting Information.

Optical Spectra. While $Li_{0.1}MoS_2$ is efficiently exfoliated in an ethanol−water mixture,[41] this method was not effective with $Li_{0.35}WS_2$. Systematic studies of $Li_{0.35}WS_2$ were carried using sodium cholate/water solutions, which have shown much higher efficiency, relative to ethanol−water, for liquid phase exfoliation of pristine TMDs.[27,48,49] Briefly, the samples were first kept under 2 h of sonication in aqueous surfactant solutions by using a horn sonicator, and the residual bulk crystals were removed by a standard centrifugation procedure.[39] UV−vis absorption spectroscopy of the supernatant shows the characteristic A-exciton peak of exfoliated 2H-WS_2 in both the $Li_{0.35}WS_2$ sample and the WS_2 control, despite their noticeable difference in absorption intensity and curve configuration (Figure 2a). Coleman and co-workers proposed that the concentration of exfoliated WS_2 nanosheets could be estimated with the local minimum of extinction spectra at ∼295 nm in the UV−vis spectrum.[50] Based on this metric, a significant increase in the yield of the exfoliated WS_2 nanosheets can be observed in the $Li_{0.35}WS_2$ sample when compared with the WS_2 control. Furthermore, the $Li_{0.35}WS_2$ suspension displays a distinct blue-shift of the A transitions, indicating that thinner nanosheets were obtained.

To enrich the fraction of single- and few-layer products, the centrifugation speed was optimized. Figure 2b shows normalized UV−vis spectra of $Li_{0.35}WS_2$ suspensions after centrifugation at different speeds. A successive blue-shift of the A-exciton from 628 to 621 nm can be obviously detected when the speed increases from 1000 to 6000 rpm. According to the empirical equation[51] that correlates the A-exciton peak and the average layer numbers (N_{avg}) of WS_2, the N_{avg} of WS_2 nanosheets in the dispersions after centrifugation at a speed of 4000−6000 rpm is close to 1. The corresponding concentrations measured by vacuum drying methods (after subtraction of the surfactant content) are in the range of 2.35 to 4 mg mL^{-1}. Thus, the yield of suspended WS_2 nanosheets was calculated to be 18−22 wt %, by taking the initial concentration of the starting WS_2 crystals into account (15 mg mL^{-1}). Note that the yield here is at least 1 order of magnitude greater than those in previous reports of WS_2 exfoliation.[27] Interestingly, a gradual decrease of the extinction coefficient at 295 nm was observed with increasing centrifugation speed. Similar

DOI: 10.1021/acsami.7b15614
ACS Appl. Mater. Interfaces 2018, 10, 2810−2818

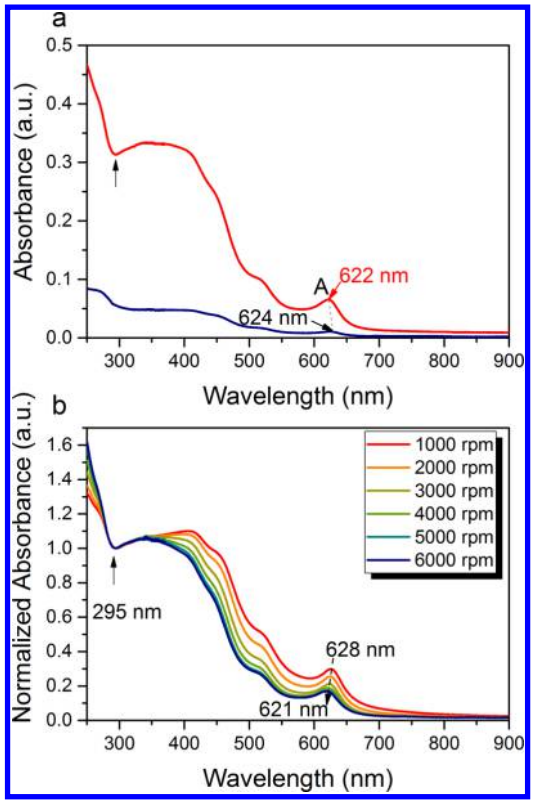

Figure 2. (a) UV−vis spectra of $Li_{0.35}WS_2$ (red line) and pristine WS_2 (blue line) suspensions. Note that the suspensions were diluted for comparison. Both $Li_{0.35}WS_2$ and WS_2 had an initial concentration of 15 mg mL^{-1}, and the samples were subjected to sonication of 2 h (40% × 700 W) prior to 30 min of centrifugation at 4000 rpm. The positions of the A-excitons are marked. (b) UV−vis spectra are normalized to the absorbance at 295 nm. $Li_{0.35}WS_2$ dispersions were obtained under optimized conditions with a starting $Li_{0.35}WS_2$ concentration of 15 mg mL^{-1}. The suspensions were sonicated for 2 h (40% × 700 W) and centrifuged from 1000 to 6000 rpm for 30 min.

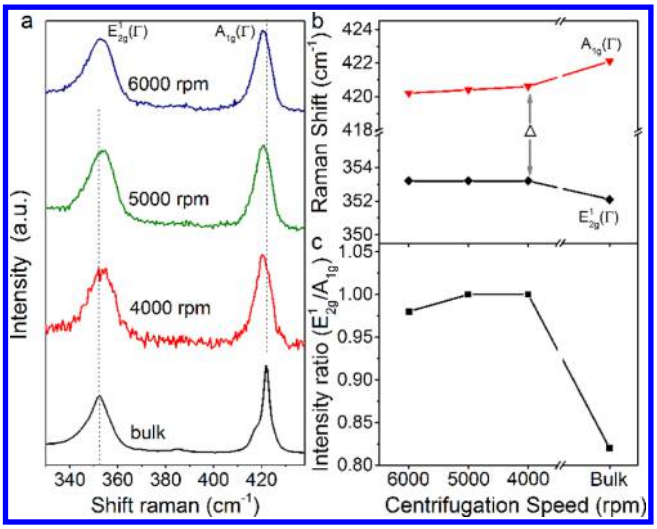

Figure 3. (a) Raman spectra of samples collected at various centrifugation speeds and normalized to the intensity of A_{1g} peak, including that from the bulk with 633 nm laser line, displaying the two characteristic E^1_{2g} and A_{1g} modes. Each spectrum was acquired under the same conditions of laser power and collection time. (b) Raman shift plotted as the difference (Δ) between the E^1_{2g} and A_{1g} mode frequencies and (c) peak intensity ratio for two characteristic peaks of E^1_{2g} and A_{1g} modes as a function of centrifugation speed, including those from bulk WS_2.

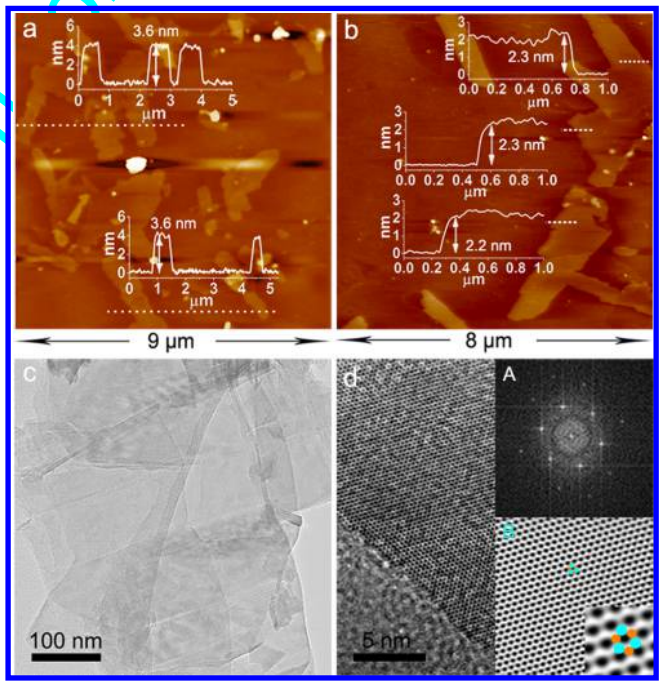

Figure 4. AFM images on a Si substrate with the cross-sectional analysis of the prepared nanosheets (a and b). (c) Typical TEM images of exfoliated WS_2 nanosheets. (d) High-resolution TEM image. Inset shows the FFT and inverse FFT patterns (scale bar = 2 nm) with individual W (green dots) and S (yellow dots) atoms and their honeycomb arrangement in a blown up image.

phenomena have been observed in MoS_2 exfoliation and may be attributed to the increased transparency of thinner and smaller nanosheets.[39,50]

Raman spectra (633 nm laser) of the exfoliated WS_2 nanosheets show the characteristic E^1_{2g} (in-plane phonon) and A_{1g} (out-of-plane phonon) modes of 2H-WS_2 (Figure 3a). Compared with bulk WS_2 crystals, the exfoliated WS_2 samples (after centrifugation at 4000−6000 rpm) show a red shift of the A_{1g} peak and an obvious blue shift of the E^1_{2g} peak. As shown in Figure 3b, the difference (Δ) between the E^1_{2g} and A_{1g} frequencies of these samples obviously decreases (~3 cm^{-1} smaller than in bulk WS_2 crystals). In addition, the peak intensity ratio of the E^1_{2g} to A_{1g} modes significantly increases in exfoliated WS_2 (Figure 3c). These results can be explained by the fact that the E^1_{2g} and A_{1g} modes have a well-defined thickness dependence.[52,53] Note that a 1.3−3.9 cm^{-1} decrease in the difference (Δ) between the E^1_{2g} and A_{1g} frequencies was observed in 1−2 layer WS_2 nanosheets,[54] suggesting a 1−2 layered nature of the WS_2 nanosheets obtained in our study, as discussed below.

Nanosheet Morphology. The specific layer numbers and sizes of the nanosheets obtained after centrifugation at 4000 rpm were evaluated by atomic force microscopy (AFM). In Figure 4a,b, despite the presence of many small fragments, abundant larger nanosheets with lateral dimensions of 0.2 to 1.5 μm can be readily observed. Importantly, most of these larger nanosheets (~75%; Figure S8−15 for details) have an apparent AFM height of ~2.2 or 3.6 nm. According to previous detailed studies by Coleman et al.,[36,50] the averaged layer number of these WS_2 nanosheets can be estimated to be 1−2 layers. It should be noted that the deviation of the apparent AFM height

DOI: 10.1021/acsami.7b15614
ACS Appl. Mater. Interfaces 2018, 10, 2810−2818

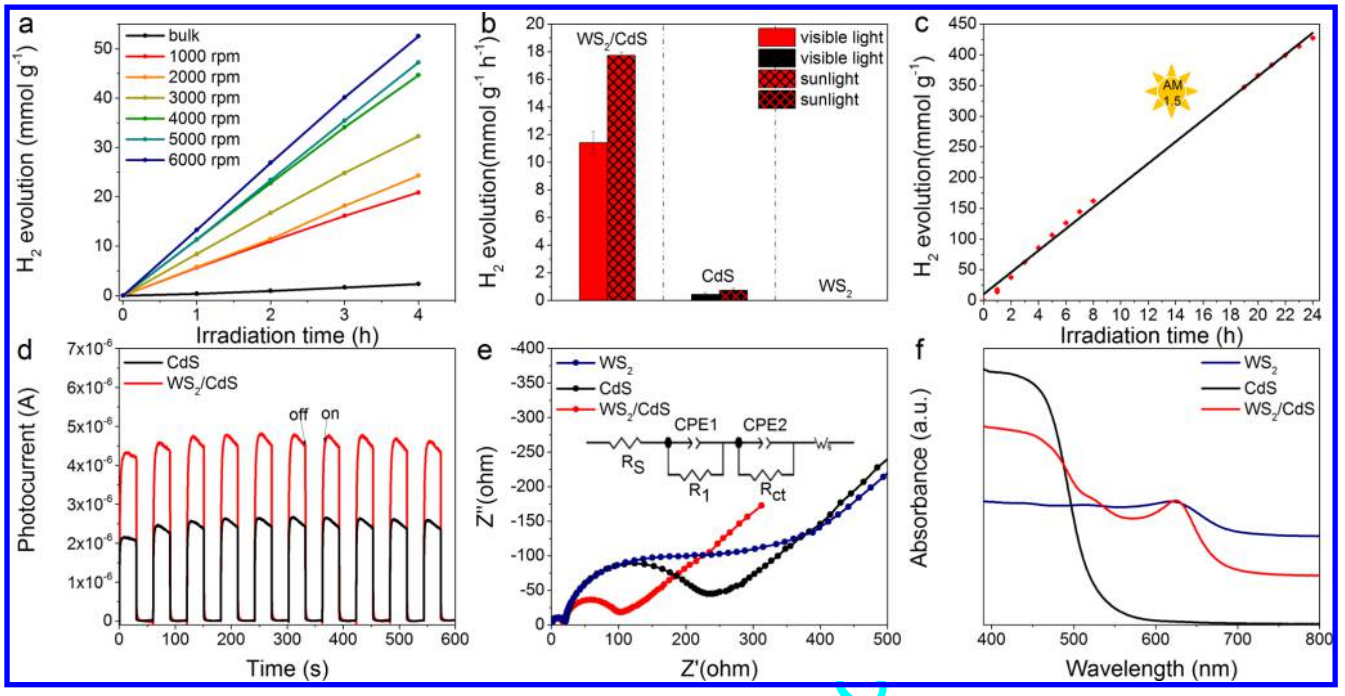

Figure 5. (a) Photocatalytic H_2 generation from WS_2/CdS NRs with nanosheets prepared by centrifugation rates between 1000 and 6000 rpm. A Xe lamp (300 W) with L42 cutoff was used as the light source in 20 vol% lactate solution (100 mL) with 50 mg catalyst. (b) The hydrogen evolution rate of different photocatalysts under visible light and simulated sunlight. (c) Photocatalytic H_2 generation from WS_2/CdS NRs during irradiation under simulated sunlight at AM 1.5. (d) Transient photocurrent response and (e) electrochemical impedance spectra (EIS) of electrodes consisting of CdS NRs, exfoliated WS_2 and WS_2/CdS nanohybrids. The inset displays an equivalent circuit applied to model the EIS result.[63,64] (f) Diffuse reflectance UV−vis spectra of CdS, WS_2, and WS_2/CdS.

from the theoretical thickness can be explained by the intrinsic out-of-plane deformation of two-dimensional nanosheets, as well as by the possible presence of trapped solvent or surfactant.[34,50] These results are in line with the empirical UV−vis results (N_{avg} of 1−2) described above.

As shown in Figure 4c, the WS_2 nanosheets appear transmissive to electrons, despite their heavy stacking on the TEM grids. Moreover, an obvious hexagonal lattice can be readily observed in high-resolution TEM (Figure 4d) and the fast Fourier transform (FFT) pattern (inset A in Figure 4d). After inverse FFT filtering of the TEM image, inset B in Figure 4d shows the 2H honeycomb structure of WS_2, in which differences in their contrast can be used to identify W and S sites easily. These results indicate the successful preparation of 2H-WS_2 nanosheets with a high degree of crystallinity.

Photocatalytic H_2 Evolution. As WS_2/CdS has been demonstrated to be a promising composite for the photocatalytic H_2 evolution reaction,[45,55,56] we further investigated the performance of our exfoliated WS_2 nanosheets as non-noble metal cocatalyst for HER of CdS. Considering that CdS nanorods (NRs) show much better performance than conventional nanoparticles,[57,58] the WS_2/CdS NRs hybrids were constructed by mixing the WS_2 nanosheets with CdS nanorods (NRs; Figure S16) in different mass ratios. A preliminary investigation revealed that an optimized hybrid with 8 wt % WS_2 nanosheets showed the highest H_2 evolution rate (Figure S17) when lactate was used as a sacrificial electron donor. To evaluate the influence of the layer number on the catalytic performance of the WS_2/CdS NRs hybrids (8 wt % WS_2), WS_2 nanosheets that were centrifuged at different speeds were mixed with CdS nanorods (NRs), and the hybrids were systematically compared (Figure 5a). Note that the CdS NRs alone have limited H_2 evolution activity, whereas the exfoliated WS_2 nanosheets are inert for the photocatalytic reaction (Figure 5b). As expected, the hybrid with bulk WS_2 crystals shows hardly any activity for the HER during visible light irradiation. In contrast, the cocatalytic activity of WS_2 nanosheets increased with increasing centrifugation speed, indicating that the thinner and smaller WS_2 nanosheets are more active. Notably, the hybrid with WS_2 nanosheets centrifuged at >4000 rpm showed a sudden rise in activity, in concert with the result that most of these WS_2 nanosheets are 1−2 layers thick. The H_2 evolution rate of this hybrid under visible light and simulated sunlight are 11.41 and 17.73 mmol h^{-1} g^{-1}, respectively. These values are about 26-fold higher than that obtained with bare CdS NRs under the same conditions, and an absorbed photon quantum yield (AQE) of 67% was observed at 420 nm (Figure S16). Note that the AQE of the WS_2/CdS NRs hybrid here is comparable to the best counterpart which involves single layer WS_2[45] and that it is obviously better than the other hybrids used in previous studies.[55,56,59] As summarized in Table S2, previous studies have showed that the thinner the WS_2 nanosheets involved, the higher the AQE of the hybrids. This suggests that the high AQE found here can be attributed to the abundant 1−2 layered WS_2 nanosheets, which have much higher AQE than bulk or few-layer WS_2.[60] It should be noted that the activities of the CdS/WS_2 composite depend on not only the synergistic effect between CdS and WS_2 but also the intrinsic activities of the CdS. Besides, the different sizes and phases of the WS_2 should also affect the synergistic catalysis of CdS and WS_2. That may explain the relatively lower hydrogen evolution rate of the CdS/WS_2 composite here when compared with the state-of-art CdS/WS_2 composite.[55,56] Moreover, there is no obvious decrease in the H_2 evolution rate after irradiation for 24 h, indicating good stability of the photocatalysts (Figure 5c). Photoelectrochemical measurements revealed that the

DOI: 10.1021/acsami.7b15614
ACS Appl. Mater. Interfaces 2018, 10, 2810−2818

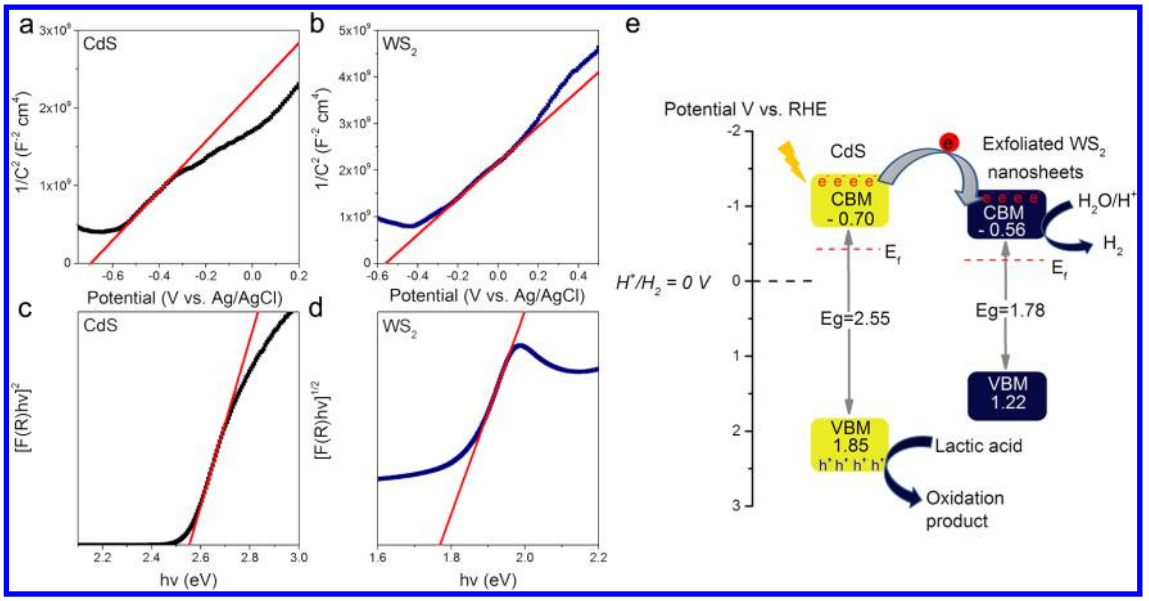

Figure 6. Mott–Schottky plots of (a) CdS NRs with E_{fb} of about −0.70 V and (b) exfoliated WS_2 with E_{fb} of about −0.56 V vs Ag/AgCl, from the intercepts of the plots on the potential axis. These values can be converted into −0.40 V for bare CdS NRs and −0.26 V for WS_2 nanosheets vs RHE, respectively. (c) The Kubelka–Munk plot vs photon energy for CdS NRs. The energy value at the point of intersection of the tangent line and the horizontal axis is the band gap (energy band gap of CdS NRs: ∼2.55 eV). The indirect band gap of WS_2 nanosheets is ∼1.78 eV (d). (e) Energy level of CdS and exfoliated 2H-WS_2.

WS_2/CdS NR hybrid gave approximately twice the photocurrent when compared with unmodified CdS NRs (Figure 5d). Electrochemical impedance spectroscopy (EIS) measurements (Figure 5e) confirmed that the hybrids had a much smaller R_{ct} (charge transfer resistance) in comparison with bare WS_2 and CdS NRs. It is known that a smaller R_{ct} means more effective charge transfer across interfaces between electrode and electrolyte.[61,62] In UV–vis diffuse reflectance spectra (Figure 5f), the absorbance of the WS_2/CdS NRs hybrid in visible regions obviously increases, and the characteristic high absorbance of 1–2 layered WS_2 is apparent in the visible region, both of which contribute to the photocatalytic activity. However, the 1–2 layer WS_2 nanosheets alone are inert for the photocatalytic reaction (Figure 5b). Therefore, we can conclude that the significant increase in the H_2 evolution rate of the WS_2/CdS hybrids can be mainly due to the synergistic effect between WS_2 nanosheets and CdS.

To probe the mechanisms involved, Mott–Schottky analyses of the CdS NRs and WS_2 nanosheets were performed under dark conditions to estimate the flat band potential (E_{fb}). As seen in Figure 6a,b, the Mott–Schottky plots show positive slopes, demonstrating that both bare CdS NRs and WS_2 nanosheets have n-type semiconducting properties with flat-band potentials (E_{fb}) of about −0.70 and −0.56 V vs Ag/AgCl, respectively. In general, for n-type semiconductors, it is known that E_{fb} values measured by the Mott–Schottky method are about 0.3 V positive of the conduction-band minimum (CBM).[65−69] Thus the CBM of the CdS NRs and the WS_2 nanosheets can be estimated to be −0.70 and −0.56 V vs RHE, respectively (see the Supporting Information, eq S3). Considering that the optical band gaps of the CdS NRs and the 1–2 layered WS_2 nanosheets were measured to be 2.55 and 1.78 eV, respectively (Figure 6c,d), their energy band positions can be summarized as shown in Figure 6e. Since the estimated conduction band potential of the WS_2 nanosheets is more positive than that of the CdS NRs, electrons generated from the CdS NRs under irradiation can be transferred easily to the WS_2 nanosheets. Photogenerated holes should remain at the VBM of CdS where they are trapped by lactate ions in the solution. Therefore, the recombination between photoinduced electrons and holes can be efficiently suppressed. In addition, the Gibbs free energy of adsorbed atomic hydrogen for MoS_2 and WS_2 is close to that of catalytic precious metals like Pt,[70] and the electrons transferred from the CdS NRs to the WS_2 can thus be effectively utilized. As a consequence, more photoinduced electrons can be used to produce hydrogen, and the rate of hydrogen evolution improves.

CONCLUSION

In summary, we have successfully exfoliated WS_2 crystals into 1–2 layer 2H-WS_2 nanosheets by a modified liquid-phase exfoliation (LPE) method that involved a preintercalation step with substoichiometric *n*-butyllithium. Both DFT calculations and experimental results confirmed that the WS_2 crystals can react with *n*-butyllithium up to a stoichiometry of $Li_{0.35}WS_2$ without the undesired 2H → 1T phase change. $Li_{0.35}WS_2$ can be readily exfoliated into 1–2 layer 2H-WS_2 nanosheets with an unprecedented high yield of 18–22 wt %. The exfoliated WS_2 nanosheeets show an optical indirect band gap of ∼1.78 eV and can be used as a cocatalyst for photocatalytic hydrogen evolution. The hydrogen evolution rate was dramatically increased for the WS_2/CdS hybrids relative to their pure CdS counterpart by lowering the charge transfer resistance of the system through catalysis of the hydrogen evolution reaction.

EXPERIMENTAL SECTION

Density Functional Theory Calculations. All density functional theory (DFT) computations were performed using CASTEP.[71] A cutoff energy of 450 eV was used for plane-wave basis set. The electron exchange-correlation energy was described by the general gradient approximation (GGA) in the Perdew–Burke–Ernzerh (PBE) exchange-correlation functional.[72] The semiempirical method proposed by Grimme[73,74] was used to account for the van der Waals interaction in WS_2. The geometry optimizations were performed using

DOI: 10.1021/acsami.7b15614
ACS Appl. Mater. Interfaces 2018, 10, 2810–2818

the conjugated gradient algorithm with a convergence threshold of 2.0 × 10^{-5} eV/atom for energy and 0.05 eV/Å for force. The Brillouin zone was represented by Monkhorst−Pack grids with a spacing of 0.05 $Å^{-1}$. All calculations were spin-polarized. More explanations are given in the Supporting Information.

Preintercalation and Exfoliation of 2H-WS_2. Microcrystals of WS_2 (2 μm 99.9%, Aladdin) were intercalated by adding a controlled amount of *n*-butyllithium (2.5 M in hexane, SPC scientific) at 50 °C. In detail, for the $Li_{0.35}WS_2$, 6.199 g of WS_2 was mixed with 40 mL of hexanes that included 8.75 mmol *n*-butyllithium under Ar atmosphere at 50 °C for 3 days. Then 30 mL of hexanes was used to wash the obtained compound three times and then drying in a vacuum oven at room temperature overnight.

The resulting preintercalated compound or bulk WS_2 crystals were sonicated in sodium cholate/water solutions with a sonicator (QSONICA Q700), and then the unexfoliated crystals were removed by centrifugation. The optimized procedure to obtain 1−2 layer WS_2 nanosheets was 225 mg of $Li_{0.35}WS_2$ and 15 mL of sodium cholate/water solution (1 mg/mL) loaded in a 25 mL vial, and then subjected to 2 h of sonication (40% × 700 W). Finally, the obtained dispersion was centrifugated (4000 rpm/1467 g, 30 min), and the supernatant was collected (Figure S3). UV−vis analyses were carried out to compare the parallel results provided by dividing the raw dispersion (~15 mL) after ultrasonic treatment into equal fractions and centrifuging at various speeds. The yield was calculated by measuring the concentration of the exfoliated WS_2 nanosheets in the final dispersion via the drying method and then dividing it by the initial concentration of the starting WS_2 crystals. In short, to get the averaged concentration of WS_2, 1 mL of the dispersion was repeatedly dropped on Sn foil and dried in a vacuum oven at 60 °C. Then a microbalance was used to measure the weight difference (Figures S4−S7 for more details).

Preparation of CdS NRs and WS_2/CdS NRs Hybrids. CdS NRs were prepared according to our previous work.[75] In short, 90% ethylenediamine with $Cd(OAC)_2{\cdot}2H_2O$ (2.4 mmol) and NH_2CSNH_2 (4.8 mmol) was added to a 150 mL autoclave and reacted at 120 °C for 20 h. After cooling, the residues of organic solvent were removed, and the yellow precipitate was obtained. The precipitate was used to prepare WS_2/CdS NRs hybrids (Figure S16). The exfoliated WS_2 dispersion collected by centrifugation at 4000 rpm was washed with a 45 vol % ethanol−water solution three times and redispersed in 45 vol % ethanol−water with bath sonication for 15 min. This suspension was mixed with CdS NRs in different stoichiometric ratios, bath sonicated for 2 h, stirred overnight until dry, and dried under vacuum at room temperature overnight.

Photocatalytic Hydrogen Evolution. Photocatalytic H_2 evolution was carried out in a glass reaction cell filled with 50 mg of catalyst dispersed in 20 vol % lactate solution (100 mL). This reaction cell was connected to a closed gas system with a gas circulation pump. A xenon lamp (300 W) with a L42 cutoff filter was applied as the visible light source (λ > 420 nm). An online gas chromatograph was used to measure H_2 evolution. A series of band-pass filters was used to obtain apparent quantum efficiency (AQE) at various monochromatic wavelengths. The average light intensity was measured by a radiant power energy meter (CEAULIGHT). The detailed calculation procedure is given in the Supporting Information.

Fabrication of Film Electrodes and Photoelectrochemical Measurements. A total of 10 mg of as-synthesized CdS NRs, exfoliated WS_2, and WS_2/CdS NRs nanohybrids was added in 45 vol % ethanol−water (1 mL) and sonicated for at least 30 min. Afterward, 50 μL of the obtained colloidal solution was dropped onto the surface of a 1 cm × 1 cm pretreated F-doped SnO_2 (FTO) transparent conducting glass electrode and then dried under vacuum at 60 °C for 2 h. Photoelectrochemical measurements were carried out in a three-electrode system using a CHI 660 electrochemical workstation. The irradiation source was a solar simulator equipped with an AM 1.5G filter and 300 W Xe lamp. A light intensity meter was used to adjust and measure the output light intensity to 200 mW cm^{-2}. Counter and reference electrodes were Pt foil and Ag/AgCl, respectively, and the prepared thin film FTO electrode was used as the working electrode. Photoresponses were measured during on−off (30 s) cycling of the solar simulator for 600 s in 0.5 M Na_2SO_4. Electrochemical impedance spectroscopy (EIS) measurements were carried out under solar simulator illumination by using a redox probe of 2.5 mM $K_3[Fe(CN)_6]/K_4[Fe(CN)_6]$ (1:1) mixture in 0.1 M KCl. The voltage of measurement is open-circuit potential vs Ag/AgCl under 5 mV AC perturbation signal, and the frequency is 1 × 10^6 to 0.1 Hz. The impedance spectra were fitted by using Zview software with the equivalent circuit shown in Figure 5d. The flat-band potentials (E_{fb}) of the CdS NRs and exfoliated WS_2 were obtained from Mott−Schottky plots which were carried out in the range of −0.8 to +0.6 V upon a frequency of 50 Hz. The pH (6.23) of 0.5 M aqueous Na_2SO_4 solution was adjusted by addition of H_2SO_4 to the same pH (1.8) of 20 vol % lactic acid solution. This solution then served as the electrolyte under dark conditions for the Mott−Schottky measurements.

Characterization. Samples were characterized by a series of methods, such as UV−vis spectroscopy (UV-3802 and PerkinElmer Lambda 35), X-ray photoelectron spectroscopy (XPS, PerkinElmer, PHI 1600), atomic force microscopy (AFM, Nova Px 3.2.4 and CSPM 5000), high-resolution transmission electron microscopy (HRTEM, Philips Tecnai G2F20), Raman (NTEGRA Spectra), scanning electron microscopy (SEM, Hitachi S4800), and online gas chromatography (CEL-SPH2N).

■ ASSOCIATED CONTENT

Supporting Information

The Supporting Information is available free of charge on the ACS Publications website at DOI: 10.1021/acsami.7b15614.

Exfoliated WS_2 nanosheets were further characterized, including the details of the DFT caculations, the XPS spectrum analysis of WS_2 crystals before and after preintercalation, photographs of a nanosheets suspension and a film, additional UV−vis spectra, AFM data, details for size and thickness distributions, the low-resolution SEM and TEM images of WS_2/CdS composites and photocatalytic H_2 evolution activities. (PDF)

■ AUTHOR INFORMATION

Corresponding Authors

*E-mail: tem5@psu.edu.

*E-mail: xiaobinfan@tju.edu.cn.

ORCID

Pengtao Xu: 0000-0002-4470-446X

Wenchao Peng: 0000-0002-1515-8287

Yang Li: 0000-0003-3003-9857

Thomas E. Mallouk: 0000-0003-4599-4208

Xiaobin Fan: 0000-0002-9615-3866

Notes

The authors declare no competing financial interest.

■ ACKNOWLEDGMENTS

This study is supported by the National Natural Science Funds (Nos. 21676198 and 21403115) and the Program of Introducing Talents of Discipline to Universities (No. B06006). The authors acknowledge the National Science Foundation under Grant DMR-1306938.

■ REFERENCES

(1) Novoselov, K. S.; Fal'ko, V. I.; Colombo, L.; Gellert, P. R.; Schwab, M. G.; Kim, K. A Roadmap for Graphene. *Nature* **2012**, *490*, 192−200.

(2) Geim, A. K. Graphene: Status and Prospects. *Science* **2009**, *324*, 1530−1534.

DOI: 10.1021/acsami.7b15614
ACS Appl. Mater. Interfaces 2018, 10, 2810−2818

(3) Chhowalla, M.; Shin, H. S.; Eda, G.; Li, L. J.; Loh, K. P.; Zhang, H. The Chemistry of Two-Dimensional Layered Transition Metal Dichalcogenide Nanosheets. *Nat. Chem.* **2013**, *5*, 263−275.
(4) Xu, M.; Liang, T.; Shi, M.; Chen, H. Graphene-Like Two-Dimensional Materials. *Chem. Rev.* **2013**, *113*, 3766−3798.
(5) Tan, C.; Cao, X.; Wu, X. J.; He, Q.; Yang, J.; Zhang, X.; Chen, J.; Zhao, W.; Han, S.; Nam, G. H.; Sindoro, M.; Zhang, H. Recent Advances in Ultrathin Two-Dimensional Nanomaterials. *Chem. Rev.* **2017**, *117*, 6225−6331.
(6) Huang, X.; Zeng, Z.; Zhang, H. Metal Dichalcogenide Nanosheets: Preparation, Properties and Applications. *Chem. Soc. Rev.* **2013**, *42*, 1934−1946.
(7) Khalil, H. M.; Khan, M. F.; Eom, J.; Noh, H. Highly Stable and Tunable Chemical Doping of Multilayer WS_2 Field Effect Transistor: Reduction in Contact Resistance. *ACS Appl. Mater. Interfaces* **2015**, *7*, 23589−23596.
(8) Wang, Q. H.; Kalantar-Zadeh, K.; Kis, A.; Coleman, J. N.; Strano, M. S. Electronics and Optoelectronics of Two-Dimensional Transition Metal Dichalcogenides. *Nat. Nanotechnol.* **2012**, *7*, 699−712.
(9) Chia, X.; Eng, A. Y.; Ambrosi, A.; Tan, S. M.; Pumera, M. Electrochemistry of Nanostructured Layered Transition-Metal Dichalcogenides. *Chem. Rev.* **2015**, *115*, 11941−11966.
(10) Shim, J.; Park, H.; Kang, D.; Kim, J.; Jo, S.; Park, Y.; Park, J. Electronic and Optoelectronic Devices based on Two-Dimensional Materials: From Fabrication to Application. *Adv. Electron. Mater.* **2017**, *3*, 1600364−1600389.
(11) Tan, H.; Fan, Y.; Zhou, Y.; Chen, Q.; Xu, W.; Warner, J. H. Ultrathin 2D Photodetectors Utilizing Chemical Vapor Deposition Grown WS_2 With Graphene Electrodes. *ACS Nano* **2016**, *10*, 7866−7873.
(12) Kim, K. S.; Kim, K. H.; Nam, Y.; Jeon, J.; Yim, S.; Singh, E.; Lee, J. Y.; Lee, S. J.; Jung, Y. S.; Yeom, G. Y.; Kim, D. W. Atomic Layer Etching Mechanism of MoS_2 for Nanodevices. *ACS Appl. Mater. Interfaces* **2017**, *9*, 11967−11976.
(13) Tanabe, I.; Gomez, M.; Coley, W. C.; Le, D.; Echeverria, E. M.; Stecklein, G.; Kandyba, V.; Balijepalli, S. K.; Klee, V.; Nguyen, A. E.; Preciado, E.; Lu, I. H.; Bobek, S.; Barroso, D.; Martinez-Ta, D.; Barinov, A.; Rahman, T. S.; Dowben, P. A.; Crowell, P. A.; Bartels, L. Band Structure Characterization of WS_2 Grown by Chemical Vapor Deposition. *Appl. Phys. Lett.* **2016**, *108*, 252103−252107.
(14) Deng, D.; Novoselov, K. S.; Fu, Q.; Zheng, N.; Tian, Z.; Bao, X. Catalysis with Two-Dimensional Materials and Their Heterostructures. *Nat. Nanotechnol.* **2016**, *11*, 218−230.
(15) Zhang, Y.; Shi, J.; Han, G.; Li, M.; Ji, Q.; Ma, D.; Zhang, Y.; Li, C.; Lang, X.; Zhang, Y.; Liu, Z. Chemical Vapor Deposition of Monolayer WS_2 Nanosheets on Au Foils toward Direct Application in Hydrogen Evolution. *Nano Res.* **2015**, *8*, 2881−2890.
(16) Dong, H.; Chen, D.; Wang, K.; Zhang, R. High-Yield Preparation and Electrochemical Properties of Few-Layer MoS_2 Nanosheets by Exfoliating Natural Molybdenite Powders Directly via a Coupled Ultrasonication-Milling Process. *Nanoscale Res. Lett.* **2016**, *11*, 409−423.
(17) Fan, X.; Xu, P.; Zhou, D.; Sun, Y.; Li, Y. C.; Nguyen, M. A.; Terrones, M.; Mallouk, T. E. Fast and Efficient Preparation of Exfoliated 2H MoS_2 Nanosheets by Sonication-Assisted Lithium Intercalation and Infrared Laser-Induced 1T to 2H Phase Reversion. *Nano Lett.* **2015**, *15*, 5956−5960.
(18) Eda, G.; Yamaguchi, H.; Voiry, D.; Fujita, T.; Chen, M.; Chhowalla, M. Photoluminescence from Chemically Exfoliated MoS_2. *Nano Lett.* **2011**, *11*, 5111−5117.
(19) Miremadi, B. K.; Morrison, S. R. The Intercalation and Exfoliation of Tungsten Disulfide. *J. Appl. Phys.* **1988**, *63*, 4970−4974.
(20) Voiry, D.; Yamaguchi, H.; Li, J.; Silva, R.; Alves, D. C.; Fujita, T.; Chen, M.; Asefa, T.; Shenoy, V. B.; Eda, G.; Chhowalla, M. Enhanced Catalytic Activity in Strained Chemically Exfoliated WS_2 Nanosheets for Hydrogen Evolution. *Nat. Mater.* **2013**, *12*, 850−855.
(21) Voiry, D.; Mohite, A.; Chhowalla, M. Phase Engineering of Transition Metal Dichalcogenides. *Chem. Soc. Rev.* **2015**, *44*, 2702−2714.
(22) Lin, Y. C.; Dumcenco, D. O.; Huang, Y. S.; Suenaga, K. Atomic Mechanism of the Semiconducting-to-Metallic Phase Transition in Single-Layered MoS_2. *Nat. Nanotechnol.* **2014**, *9*, 391−396.
(23) Kumar, A.; Ahluwalia, P. K. A First Principle Comparative Study of Electronic and Optical Properties of 1H − MoS_2 and 2H − MoS_2. *Mater. Chem. Phys.* **2012**, *135*, 755−761.
(24) Xu, D.; Zhu, Y.; Liu, J.; Li, Y.; Peng, W.; Zhang, G.; Zhang, F.; Fan, X. Microwave-Assisted 1T to 2H Phase Reversion of MoS_2 in Solution: a Fast Route to Processable Dispersions of 2H-MoS_2 Nanosheets and Nanocomposites. *Nanotechnology* **2016**, *27*, 385604−385611.
(25) Chou, S. S.; Huang, Y. K.; Kim, J.; Kaehr, B.; Foley, B. M.; Lu, P.; Dykstra, C.; Hopkins, P. E.; Brinker, C. J.; Huang, J.; Dravid, V. P. Controlling the Metal to Semiconductor Transition of MoS_2 and WS_2 in Solution. *J. Am. Chem. Soc.* **2015**, *137*, 1742−1745.
(26) Li, H.; Wu, J.; Yin, Z.; Zhang, H. Preparation and Applications of Mechanically Exfoliated Single-Layer and Multilayer MoS_2 and WSe_2 Nanosheets. *Acc. Chem. Res.* **2014**, *47*, 1067−1075.
(27) Coleman, J. N.; Lotya, M.; O'Neill, A.; Bergin, S. D.; King, P. J.; Khan, U.; Young, K.; Gaucher, A.; De, S.; Smith, R. J.; Shvets, I. V.; Arora, S. K.; Stanton, G.; Kim, H. Y.; Lee, K.; Kim, G. T.; Duesberg, G. S.; Hallam, T.; Boland, J. J.; Wang, J. J.; Donegan, J. F.; Grunlan, J. C.; Moriarty, G.; Shmeliov, A.; Nicholls, R. J.; Perkins, J. M.; Grieveson, E. M.; Theuwissen, K.; McComb, D. W.; Nellist, P. D.; Nicolosi, V. Two-Dimensional Nanosheets Produced by Liquid Exfoliation of Layered Materials. *Science* **2011**, *331*, 568−571.
(28) Jawaid, A.; Nepal, D.; Park, K.; Jespersen, M.; Qualley, A.; Mirau, P.; Drummy, L. F.; Vaia, R. A. Mechanism for Liquid Phase Exfoliation of MoS_2. *Chem. Mater.* **2016**, *28*, 337−348.
(29) Varrla, E.; Backes, C.; Paton, K. R.; Harvey, A.; Gholamvand, Z.; McCauley, J.; Coleman, J. N. Large-Scale Production of Size-Controlled MoS_2 Nanosheets by Shear Exfoliation. *Chem. Mater.* **2015**, *27*, 1129−1139.
(30) Paton, K. R.; Varrla, E.; Backes, C.; Smith, R. J.; Khan, U.; O'Neill, A.; Boland, C.; Lotya, M.; Istrate, O. M.; King, P.; Higgins, T.; Barwich, S.; May, P.; Puczkarski, P.; Ahmed, I.; Moebius, M.; Pettersson, H.; Long, E.; Coelho, J.; O'Brien, S. E.; McGuire, E. K.; Sanchez, B. M.; Duesberg, G. S.; McEvoy, N.; Pennycook, T. J.; Downing, C.; Crossley, A.; Nicolosi, V.; Coleman, J. N. Scalable Production of Large Quantities of Defect-Free Few-Layer Graphene by Shear Exfoliation in Liquids. *Nat. Mater.* **2014**, *13*, 624−630.
(31) Shen, J.; He, Y.; Wu, J.; Gao, C.; Keyshar, K.; Zhang, X.; Yang, Y.; Ye, M.; Vajtai, R.; Lou, J.; Ajayan, P. M. Liquid Phase Exfoliation of Two-Dimensional Materials by Directly Probing and Matching Surface Tension Components. *Nano Lett.* **2015**, *15*, 5449−5454.
(32) Backes, C.; Higgins, T. M.; Kelly, A.; Boland, C.; Harvey, A.; Hanlon, D.; Coleman, J. N. Guidelines for Exfoliation, Characterization and Processing of Layered Materials Produced by Liquid Exfoliation. *Chem. Mater.* **2017**, *29*, 243−255.
(33) Cunningham, G.; Lotya, M.; Cucinotta, C. S.; Sanvito, S.; Bergin, S. D.; Menzel, R.; Shaffer, M. S.; Coleman, J. N. Solvent Exfoliation of Transition Metal Dichalcogenides: Dispersibility of Exfoliated Nanosheets Varies Only Weakly Between Compounds. *ACS Nano* **2012**, *6*, 3468−3480.
(34) O'Neill, A.; Khan, U.; Coleman, J. N. Preparation of High Concentration Dispersions of Exfoliated MoS_2 with Increased Flake Size. *Chem. Mater.* **2012**, *24*, 2414−2421.
(35) Zheng, J.; Zhang, H.; Dong, S.; Liu, Y.; Nai, C. T.; Shin, H. S.; Jeong, H. Y.; Liu, B.; Loh, K. P. High Yield Exfoliation of Two-Dimensional Chalcogenides Using Sodium Naphthalenide. *Nat. Commun.* **2014**, *5*, 2995−3802.
(36) Smith, R. J.; King, P. J.; Lotya, M.; Wirtz, C.; Khan, U.; De, S.; O'Neill, A.; Duesberg, G. S.; Grunlan, J. C.; Moriarty, G.; Chen, J.; Wang, J.; Minett, A. I.; Nicolosi, V.; Coleman, J. N. Large-Scale Exfoliation of Inorganic Layered Compounds in Aqueous Surfactant Solutions. *Adv. Mater.* **2011**, *23*, 3944−3948.
(37) Guan, G.; Zhang, S.; Liu, S.; Cai, Y.; Low, M.; Teng, C. P.; Phang, I. Y.; Cheng, Y.; Duei, K. L.; Srinivasan, B. M.; Zheng, Y.; Zhang, Y. W.; Han, M. Y. Protein Induces Layer-by-Layer Exfoliation

DOI: 10.1021/acsami.7b15614
ACS Appl. Mater. Interfaces 2018, 10, 2810−2818

of Transition Metal Dichalcogenides. *J. Am. Chem. Soc.* **2015**, *137*, 6152−6155.
(38) Biswas, Y.; Dule, M.; Mandal, T. K. Poly(ionic liquid)-Promoted Solvent-Borne Efficient Exfoliation of MoS_2/$MoSe_2$ Nanosheets for Dual-Responsive Dispersion and Polymer Nanocomposites. *J. Phys. Chem. C* **2017**, *121*, 4747−4759.
(39) Fan, X.; Xu, P.; Li, Y. C.; Zhou, D.; Sun, Y.; Nguyen, M. A.; Terrones, M.; Mallouk, T. E. Controlled Exfoliation of MoS_2 Crystals into Trilayer Nanosheets. *J. Am. Chem. Soc.* **2016**, *138*, 5143−5149.
(40) Jawaid, A.; Che, J.; Drummy, L. F.; Bultman, J.; Waite, A.; Hsiao, M. S.; Vaia, R. A. Redox Exfoliation of Layered Transition Metal Dichalcogenides. *ACS Nano* **2017**, *11*, 635−646.
(41) Peng, J.; Wu, J.; Li, X.; Zhou, Y.; Yu, Z.; Guo, Y.; Wu, J.; Lin, Y.; Li, Z.; Wu, X.; Wu, C.; Xie, Y. Very Large-Sized Transition Metal Dichalcogenides Monolayers from Fast Exfoliation by Manual Shaking. *J. Am. Chem. Soc.* **2017**, *139*, 9019−9025.
(42) Anto Jeffery, A.; Nethravathi, C.; Rajamathi, M. Two-Dimensional Nanosheets and Layered Hybrids of MoS_2 and WS_2 through Exfoliation of Ammoniated MS_2 (M = Mo,W). *J. Phys. Chem. C* **2014**, *118*, 1386−1396.
(43) Mahler, B.; Hoepfner, V.; Liao, K.; Ozin, G. A. Colloidal Synthesis of 1T-WS_2 and 2H-WS_2 Nanosheets: Applications for Photocatalytic Hydrogen Evolution. *J. Am. Chem. Soc.* **2014**, *136*, 14121−14127.
(44) Peng, W.; Li, Y.; Zhang, F.; Zhang, G.; Fan, X. Roles of Two-Dimensional Transition Metal Dichalcogenides as Cocatalysts in Photocatalytic Hydrogen Evolution and Environmental Remediation. *Ind. Eng. Chem. Res.* **2017**, *56*, 4611−4626.
(45) Hai, X.; Chang, K.; Pang, H.; Li, M.; Li, P.; Liu, H.; Shi, L.; Ye, J. Engineering the Edges of MoS_2 (WS_2) Crystals for Direct Exfoliation into Monolayers in Polar Micromolecular Solvents. *J. Am. Chem. Soc.* **2016**, *138*, 14962−14969.
(46) Chang, K.; Hai, X.; Pang, H.; Zhang, H.; Shi, L.; Liu, G.; Liu, H.; Zhao, G.; Li, M.; Ye, J. Targeted Synthesis of 2H- and 1T-Phase MoS_2 Monolayers for Catalytic Hydrogen Evolution. *Adv. Mater.* **2016**, *28*, 10033−10041.
(47) YANG, D.; FRINDT, R. F. Li-intercalation and Exfoliation of WS_2. *J. Phys. Chem. Solids* **1996**, *57*, 1113−1116.
(48) Zhou, K. G.; Mao, N. N.; Wang, H. X.; Peng, Y.; Zhang, H. L. A Mixed-Solvent Strategy for Efficient Exfoliation of Inorganic Graphene Analogues. *Angew. Chem., Int. Ed.* **2011**, *50*, 10839−10842.
(49) Nicolosi, V.; Chhowalla, M.; Kanatzidis, M. G.; Strano, M. S.; Coleman, J. N. Liquid Exfoliation of Layered Materials. *Science* **2013**, *340*, 1226419−1226419.
(50) Backes, C.; Smith, R. J.; McEvoy, N.; Berner, N. C.; McCloskey, D.; Nerl, H. C.; O'Neill, A.; King, P. J.; Higgins, T.; Hanlon, D.; Scheuschner, N.; Maultzsch, J.; Houben, L.; Duesberg, G. S.; Donegan, J. F.; Nicolosi, V.; Coleman, J. N. Edge and Confinement Effects Allow *in Situ* Measurement of Size and Thickness of Liquid-Exfoliated Nanosheets. *Nat. Commun.* **2014**, *5*, 4576−4586.
(51) Backes, C.; Szydlowska, B. M.; Harvey, A.; Yuan, S.; Vega-Mayoral, V.; Davies, B. R.; Zhao, P. L.; Hanlon, D.; Santos, E. J.; Katsnelson, M. I.; Blau, W. J.; Gadermaier, C.; Coleman, J. N. Production of Highly Monolayer Enriched Dispersions of Liquid-Exfoliated Nanosheets by Liquid Cascade Centrifugation. *ACS Nano* **2016**, *10*, 1589−1601.
(52) Chakraborty, B.; Matte, H. S. S. R.; Sood, A. K.; Rao, C. N. R. Layer-Dependent Resonant Raman Scattering of a Few Layer MoS_2. *J. Raman Spectrosc.* **2013**, *44*, 92−96.
(53) Lee, C.; Yan, H.; Brus, L. E.; Heinz, T. F.; Hone, J.; Ryu, S. Anomalous Lattice Vibrations of Single- and Few-Layer MoS_2. *ACS Nano* **2010**, *4*, 2695−2700.
(54) Berkdemir, A.; Gutierrez, H. R.; Botello-Mendez, A. R.; Perea-Lopez, N.; Elias, A. L.; Chia, C. I.; Wang, B.; Crespi, V. H.; Lopez-Urias, F.; Charlier, J. C.; Terrones, H.; Terrones, M. Identification of Individual and Few Layers of WS_2 Using Raman Spectroscopy. *Sci. Rep.* **2013**, *3*, 1755−1763.
(55) Gopannagari, M.; Kumar, D. P.; Reddy, D. A.; Hong, S.; Song, M. I.; Kim, T. K. *In Situ* Preparation of Few-Layered WS_2 Nanosheets and Exfoliation into Bilayers on CdS Nanorods for Ultrafast Charge Carrier Migrations toward Enhanced Photocatalytic Hydrogen Production. *J. Catal.* **2017**, *351*, 153−160.
(56) He, J.; Chen, L.; Yi, Z. Q.; Au, C. T.; Yin, S. F. CdS Nanorods Coupled with WS_2 Nanosheets for Enhanced Photocatalytic Hydrogen Evolution Activity. *Ind. Eng. Chem. Res.* **2016**, *55*, 8327−8333.
(57) Yin, X.; He, G.; Sun, B.; Jiang, W.; Xue, D.; Xia, A.; Wan, L.; Hu, J. Rational Design and Electron Transfer Kinetics of MoS_2/CdS Nanodots-on-Nanorods for Efficient Visible-Light-Driven Hydrogen Generation. *Nano Energy* **2016**, *28*, 319−329.
(58) Yin, X. L.; Li, L. L.; Jiang, W. J.; Zhang, Y.; Zhang, X.; Wan, L. J.; Hu, J. S. MoS_2/CdS Nanosheets-on-Nanorod Heterostructure for Highly Efficient Photocatalytic H_2 Generation under Visible Light Irradiation. *ACS Appl. Mater. Interfaces* **2016**, *8*, 15258−15266.
(59) Zhong, Y.; Zhao, G.; Ma, F.; Wu, Y.; Hao, X. Utilizing Photocorrosion-Recrystallization to Prepare a Highly Stable and Efficient CdS/WS_2 Nanocomposite Photocatalyst for Hydrogen Evolution. *Appl. Catal., B* **2016**, *199*, 466−472.
(60) Mak, K. F.; Lee, C.; Hone, J.; Shan, J.; Heinz, T. F. Atomically Thin MoS_2: a New Direct-Gap Semiconductor. *Phys. Rev. Lett.* **2010**, *105*, 136805.
(61) Yu, X.; Du, R.; Li, B.; Zhang, Y.; Liu, H.; Qu, J.; An, X. Biomolecule-Assisted Self-Assembly of CdS/MoS_2/Graphene Hollow Spheres as High-Efficiency Photocatalysts for Hydrogen Evolution without Noble Metals. *Appl. Catal., B* **2016**, *182*, 504−512.
(62) Reddy, D. A.; Park, H.; Ma, R.; Kumar, D. P.; Lim, M.; Kim, T. K. Heterostructured WS_2-MoS_2 Ultrathin Nanosheets Integrated on CdS Nanorods to Promote Charge Separation and Migration and Improve Solar-Driven Photocatalytic Hydrogen Evolution. *ChemSusChem* **2017**, *10*, 1563−1570.
(63) Wang, Y.; Sun, P.; Zhao, J.; Gao, M.; Yi, Q.; Su, Y.; Gao, L.; Zou, G. A Light-Scattering Co-adsorbent for Performance Improvement of Dye-Sensitized Solar Cells. *Electrochim. Acta* **2016**, *194*, 67−73.
(64) Xu, X.; Xu, G. Electrochemical Impedance Spectra of CdSe Quantume Dots Sensitized Nanocrystalline TiO_2 Solar Cells. *Sci. China: Chem.* **2011**, *54*, 205−210.
(65) Yin, W.; Bai, L.; Zhu, Y.; Zhong, S.; Zhao, L.; Li, Z.; Bai, S. Embedding Metal in the Interface of a p-n Heterojunction with a Stack Design for Superior Z-Scheme Photocatalytic Hydrogen Evolution. *ACS Appl. Mater. Interfaces* **2016**, *8*, 23133−23142.
(66) Pi, Y.; Li, Z.; Xu, D.; Liu, J.; Li, Y.; Zhang, F.; Zhang, G.; Peng, W.; Fan, X. 1T-Phase MoS_2 Nanosheets on TiO_2 Nanorod Arrays: 3D Photoanode with Extraordinary Catalytic Performance. *ACS Sustainable Chem. Eng.* **2017**, *5*, 5175−5182.
(67) Chang, K.; Hai, X.; Ye, J. Transition Metal Disulfides as Noble-Metal-Alternative Co-Catalysts for Solar Hydrogen Production. *Adv. Energy Mater.* **2016**, *6*, 1502555−1502576.
(68) Chang, K.; Li, M.; Wang, T.; Ouyang, S.; Li, P.; Liu, L.; Ye, J. Drastic Layer-Number-Dependent Activity Enhancement in Photocatalytic H_2 Evolution over nMoS_2/CdS ($n \geq 1$) Under Visible Light. *Adv. Energy Mater.* **2015**, *5*, 1402279−1402289.
(69) Xu, P.; Milstein, T. J.; Mallouk, T. E. Flat-Band Potentials of Molecularly Thin Metal Oxide Nanosheets. *ACS Appl. Mater. Interfaces* **2016**, *8*, 11539−11547.
(70) Jaramillo, T. F.; Jorgensen, K. P.; Bonde, J.; Nielsen, J. H.; Horch, S.; Chorkendorff, I. Identification of Active Edge Sites for Electrochemical H_2 Evolution from MoS_2 Nanocatalysts. *Science* **2007**, *317*, 100−102.
(71) Clark, S. J.; Segall, M. D.; Pickard, C. J.; Hasnip, P. J.; Probert, M. I. J.; Refson, K.; Payne, M. C. First Principles Methods Using CASTEP. *Z. Kristallogr. - Cryst. Mater.* **2005**, *220*, 567−570.
(72) Perdew, J. P.; Burke, K.; Ernzerhof, M. Generalized Gradient Approximation Made Simple. *Phys. Rev. Lett.* **1996**, *77*, 3865−3868.
(73) McNellis, E. R.; Meyer, J.; Reuter, K. Azobenzene at Coinage Metal Surfaces: Role of Dispersive van der Waals Interactions. *Phys. Rev. B: Condens. Matter Mater. Phys.* **2009**, *80*, 205414−205425.
(74) Grimme, S. Semiempirical GGA-Type Density Functional Constructed with a Long-Range Dispersion Correction. *J. Comput. Chem.* **2006**, *27*, 1787−1799.

DOI: 10.1021/acsami.7b15614
ACS Appl. Mater. Interfaces 2018, 10, 2810−2818

(75) Du, P.; Zhu, Y.; Zhang, J.; Xu, D.; Peng, W.; Zhang, G.; Zhang, F.; Fan, X. Metallic 1T Phase MoS_2 Nanosheets as a Highly Efficient Co-catalyst for the Photocatalytic Hydrogen Evolution of CdS Nanorods. *RSC Adv.* **2016**, *6*, 74394−74399.

DOI: 10.1021/acsami.7b15614
ACS Appl. Mater. Interfaces 2018, 10, 2810−2818